HHS Public Access

Author manuscript

Nat Med. Author manuscript; available in PMC 2019 December 16.

Published in final edited form as:

Nat Med. 2017 December ; 23(12): 1488–1498. doi:10.1038/nm.4437.

Enhancing the precision of genetic lineage tracing using dual recombinases

Lingjuan He[1,2], **Yan Li**[1,2], **Yi Li**[1,2], **Wenjuan Pu**[1,2], **Xiuzhen Huang**[1,2], **Xueying Tian**[1,2], **Yue Wang**[1,2], **Hui Zhang**[1,2], **Qiaozhen Liu**[1,2], **Libo Zhang**[1,2], **Huan Zhao**[1,2], **Juan Tang**[1,2], **Hongbin Ji**[1,3], **Dongqing Cai**[4], **Zhibo Han**[5], **Zhongchao Han**[5], **Yu Nie**[6], **Shengshou Hu**[6], **Qing-Dong Wang**[7], **Ruilin Sun**[8], **Jian Fei**[8], **Fengchao Wang**[9], **Ting Chen**[9], **Yan Yan**[10], **Hefeng Huang**[11], **William T. Pu**[12], **Bin Zhou**[1,2,3,4,13]

[1]The State Key Laboratory of Cell Biology, CAS Center for Excellence in Molecular Cell Science, Shanghai Institute of Biochemistry and Cell Biology, Chinese Academy of Sciences, University of Chinese Academy of Sciences, Shanghai, 200031, China.

[2]Key Laboratory of Nutrition and Metabolism, Institute for Nutritional Sciences, Shanghai Institutes for Biological Sciences, Chinese Academy of Sciences, University of Chinese Academy of Sciences, Shanghai, 200031, China.

[3]School of Life Science and Technology, ShanghaiTech University, Shanghai, 201210, China.

[4]Key Laboratory of Regenerative Medicine of Ministry of Education, Institute of Aging and Regenerative Medicine, Jinan University, Guangzhou, 510632, China.

[5]The State Key Laboratory of Experimental Hematology, Institute of Hematology and Hospital of Blood Disease, Chinese Academy of Medical Science & Peking Union Medical College, Tianjin, 300020, China.

[6]State Key Laboratory of Cardiovascular Disease, Fuwai Hospital, National Center for Cardiovascular Disease, Chinese Academy of Medical Sciences and Peking Union Medical College, Beijing 100037, China.

[7]Cardiovascular and Metabolic Diseases, Innovative Medicines and Early Clinical Development Biotech Unit, AstraZeneca, Mölndal, 43183, Sweden.

[8]Shanghai Model Organisms Center, Inc., Shanghai, 201203, China.

[9]National Institute of Biological Sciences, Beijing, 102206, China.

[10]Zhongshan Hospital, Fudan University, Shanghai, 200032, China.

[11]The International Peace Maternity and Child Health Hospital, School of Medicine, Shanghai Jiao Tong University, Shanghai, China.

Correspondence should be addressed to B.Z. (zhoubin@sibs.ac.cn).

AUTHOR CONTRIBUTIONS

L.H. and B.Z. designed the study, performed experiments and analyzed the data. Y.L., Y.L., W.P., X.H., X.T., Y.W., H.Z., Q.L., L.Z., H.Z. and J.T. bred the mice and performed experiments. D.C., H.J., Z.H., Z.H., Y.N., S.H., Q.-D.W., R.S., J.F., Y.Y. and H.H. analyzed the data, technical support and edited the manuscript, F.W. and T.C. provided mouse line, W.T.P. provided intellectual input and edited the manuscript, B.Z. conceived and supervised the study, analyzed the data and wrote the manuscript.

Online content Methods, Supplementary text, Supplementary Figures 1–11 and Supplementary Table 1.

The authors declare no competing financial interests.

[12]Department of Cardiology, Boston Children's Hospital, 300 Longwood Avenue, Boston, MA 02115, and Harvard Stem Cell Institute, Harvard University, Cambridge, MA, 02138, USA.

[13]Collaborative Innovation Center of Tianjin for Medical Epigenetics, Tianjin Medical University, Tianjin, 300070, China.

Abstract

The Cre-*lox*P recombination system is the most widely used technology for *in vivo* tracing of stem or progenitor cell lineages. The precision of this genetic system largely depends on the specificity of Cre expression in targeted stem or progenitor cells. However, Cre expression in non-targeted cell types can complicate the interpretation of lineage-tracing studies and has caused controversy in many previous studies. Here we describe a new genetic lineage-tracing system that incorporates Dre-*rox* to enhance the precision of conventional Cre-*lox*P mediated lineage tracing. The Dre-*rox* recombination system permits rigorous control of potential unintentional Cre-*lox*P recombination, effectively circumventing the uncertainty of the cell-type specificity of Cre expression in lineage tracing. Using this new system, we investigated two topics of recent debates: the contribution of c-Kit$^+$ cardiac stem cells to cardiomyocytes in the heart and the contribution of Sox9$^+$ hepatic progenitor cells to hepatocytes in the liver. By overcoming the technical hurdle of non-specific Cre expression, this new technology provides a means for more precise analysis of cell lineage and fate decisions, facilitating *in vivo* study of stem and progenitor cell plasticity in disease and regeneration.

Editorial summary

Genetic cell-lineage tracing studies in mice are crucial for delineating the contribution of stem and progenitor cells to different cell types, both in disease states and after regenerative therapy. He *et al.* have developed new genetic lineage tracing systems that provide more definitive results than the commonly used Cre-based system and show that this new technology can resolve current controversies in the field, as demonstrated by lineage tracing studies in the heart and liver.

During differentiation, stem and progenitor cells make lineage choices that progressively narrow the range of cell types that can be generated, until the ultimate, differentiated cell type is formed. A cell's lineage captures its developmental trajectory from its progenitors, and a cell's fate is the differentiated cell type(s) that it will form. Unraveling cell lineage and fate determination provides fundamental information about stem cell function during development, disease and regeneration. Genetic lineage tracing is a powerful means to interrogate stem cell lineage and cell fate determination[1–6]. The most widely used technology for *in vivo* stem cell tracking uses the Cre-*lox*P recombination system[7]. In transgenic mice that express Cre within a defined population of stem cells, Cre-mediated recombination removes *lox*P-flanked transcriptional stop DNA sequences, permitting expression of a reporter gene in the Cre$^+$ cells[8]. Since this genetic labeling is irreversible and heritable, the progeny of the Cre-marked cells continue to express the reporter gene, whether or not they actively express Cre. If a Cre-marked cell differentiates into a different cell type, its expression of the genetic lineage reporter provides evidence that it belongs to the Cre-expressing lineage (Fig. 1a, scenario 1, cell type B (Cell B) is derived from cell type A (Cell A)).

Although Cre-*lox*P-based lineage tracing has provided unprecedented insights into mammalian development and into disease states, this technology has a technical hurdle that may sometimes confound interpretation of the results. The linchpin for accurate interpretation of Cre-*lox*P-based fate mapping data is precise delineation of the pattern of Cre expression[9,10], since Cre expression in non-targeted cells could lead to tracing of unintended lineages and confound interpretation of the fate mapping data. For example, expression of a gene in both Cell A and Cell B can and often does occur. Cre labeling of both Cell A and Cell B cannot be used to formally conclude that Cell A differentiates into Cell B. Rather, this type of double labeling simply makes the genetic lineage tracing experiment uninterpretable. To properly infer that Cell B is derived from Cell A, one must exclude Cre-*lox*P recombination in Cell B itself (Fig. 1a, Scenario 2, where the inference that Cell B arises from Cell A is confounded by Cre expression in Cell B). Because Cre-*lox*P recombination is sensitive, it can be technically challenging to fully exclude low level or infrequent Cre expression in non-targeted cells, creating a major hurdle for rigorous interpretation of the results of Cre-*lox*P-mediated genetic lineage tracing[10]. Here we present a new system that uses dual recombinases (Cre and Dre) and new reporter lines to resolve the unintentional lineage tracing issue and achieve more selective genetic tracing.

RESULTS

Generation of an interleaved dual reporter for exclusive recombination

To exclude genetic recombination in non-targeted cells, we generated a new genetic lineage tracing system that uses both Cre-*lox*P and Dre-*rox* recombination systems. Similar to the Cre-*lox*P system, Dre recombinase excises DNA regions flanked by *rox* recombination sites[11]. We first used mice that express these recombinases from the widely-expressed promoters ACTB and CAG (*ACTB-Cre* and *CAG-Dre*). We tested the activity and specificity of these transgenic mice using the recombinase-activated reporters *R26-loxP-tdTomato* and *R26-rox-tdTomato*. We found that the Cre and Dre recombinases specifically recognize *lox*P and *rox* respectively (Fig. 1b), consistent with a previous report[12]. Taking advantage of these orthogonal recombination systems, we generated a reporter allele in the *Rosa26* locus in which two pairs of recombination recognition sites were interleaved, such that successful Cre-*lox*P recombination activates ZsGreen, whereas successful Dre-*rox* recombination activates tdTomato (Fig. 1c). We named this *i*nterleaved *r*eporter (*IR*) mouse line *IR1*. Because the recombinase recognition sites are interleaved (*lox*P-*rox*-*lox*P-*rox*), recombination by one system (e.g., Dre-*rox*) inherently removes one recombinase recognition site of the other system (e.g., *lox*P), rendering the reporter inert to subsequent recombination (e.g., Cre-*lox*P). Thus, in Fig. 1a, Scenario 2, programming Cell B to express Dre first would preclude subsequent potential Cre-*lox*P recombination within this cell type.

To test this dual recombination system, we crossed the *IR1* line with constitutively active Dre or Cre lines (*CAG-Dre* or *ACTB-Cre*, Fig. 1d). As expected by *IR1*'s design, whole-mount fluorescence and immunostaining of sections showed that *CAG-Dre;IR1* activated expression of tdTomato but not ZsGreen, whereas *ACTB-Cre;IR1* activated expression of ZsGreen but not tdTomato (Fig. 1e,f). Similar results were obtained when *IR1* was recombined by inducible recombinases (Supplementary Fig. 1), created by fusion of the

recombinase with an engineered domain of estrogen hormone receptor (ER); the activity of these inducible recombinases is dependent upon the presence of tamoxifen[13]. We generated an inducible *CAG-DreER* allele (Supplementary Fig. 1a,b) and crossed it with *IR1* for reporter detection (Supplementary Fig. 1c). Tamoxifen induction resulted in the appearance of ZsGreen^{-}tdTomato^{+} cells in tissues of *CAG-DreER;IR1* mice, whereas no recombination was detected in mice without tamoxifen treatment (Supplementary Fig. 1d). Similarly, ZsGreen^{+}tdTomato^{-} cells were observed in tissues of *UBC-CreER;IR1* (UBC is broadly expressed in embryos following tamoxifen induction (Supplementary Fig. 1e,f). These data demonstrate that the *IR1* line is responsive to both constitutive and inducible Cre/Dre recombinases.

Constitutive Dre-*rox* recombination prevents inducible Cre-*lox*P recombination

To test if using recombination by one recombinase makes the substrate unresponsive to the second recombinase, we exposed *IR1* to constitutive Dre expression and inducible CreER expression. We reasoned that after constitutive Dre-*rox* recombination, a cell containing *IR1* would no longer undergo Cre-*lox*P recombination induced by tamoxifen. We elected to perform these proof-of-concept experiments in cardiomyocytes. We first generated a *Tnni3-Dre* allele, in which Dre is driven by regulatory elements of the cardiomyocyte specific gene troponin I3 (Supplementary Fig. 2a). *Tnni3-Dre* specifically and efficiently labeled cardiomyocytes containing *R26-rox-tdTomato* or *IR1* reporters, but not cardiomyocytes harboring the *R26-loxP-tdTomato* reporter (Supplementary Fig. 2b–e). We did not detect any *Tnni3-Dre* labeling of non-cardiomyocytes, such as endothelial cells, smooth muscle cells or fibroblasts (Supplementary Fig. 2f), demonstrating that *Tnni3-Dre* strictly targets cardiomyocytes. To test if Dre-*rox* recombination precludes further Cre-mediated recombination, we generated *Tnni3-Dre;αMHC-MerCreMer;IR1* and littermate control *αMHC-MerCreMer;IR1* mice (Supplementary Fig. 3a). In the hearts of *αMHC-MerCreMer;IR1* adult mice, tamoxifen induction of Cre-mediated recombination labeled 98.21 ± 0.45% of cardiomyocytes with ZsGreen (left panel, n = 4; Supplementary Fig. 3b,c). However, using the same tamoxifen induction strategy, we did not detect any ZsGreen^{+} cardiomyocytes in the hearts of *Tnni3-Dre;αMHC-MerCreMer;IR1* mice, and all TNNI3^{+} cardiomyocytes were tdTomato^{+} (right panel, Supplementary Fig. 3b,c). These data demonstrate that constitutive Dre recombination of *IR1* blocks further inducible Cre-*lox*P recombination in cardiomyocytes (Supplementary Fig. 3d). Thus, Dre-*rox* recombination in this newly developed system could be used to preclude potential Cre-*lox*P recombination in Dre-expressing cells (eg. Cell B, Fig. 1a, scenario 2).

Since this system relies on the dual recombinases acting on an interleaved reporter, we named it *d*ual r*e*combinase *a*ctivated *l*ineage *t*racing with *i*nterleaved *r*eporter (DeaLT-IR). After this validation of DeaLT-IR for cell labeling, we next used it to resolve some uncertainties that have arisen from the possibility of unintentional lineage tracing in studies of putative resident stem cells in the heart and liver.

Unintentional cardiomyocyte tracing by *Kit-CreER*

An important topic in the cardiovascular field is the myogenic fate of c-Kit^{+} cardiac stem cells (CSCs)[14–17]. In large part, this debate regarding the myogenic potential of CSCs

originates from the uncertain specificity of Cre expression driven by regulatory elements of the Kit gene[18,19]. Indeed, we have reported that Kit-driven Cre expression in cardiomyocytes confounds interpretation of *Kit-CreER* lineage tracing data[20]. The c-Kit$^+$ cell population consists of two subpopulations: c-Kit$^+$ cardiomyocytes and c-Kit$^+$ non-cardiomyocytes; the *Kit-CreER* allele used for lineage tracing labels both populations and does not distinguish c-Kit$^+$ non-cardiomyocytes from c-Kit$^+$ cardiomyocytes[20]. Therefore, we used DeaLT-IR to prevent unintentional c-Kit$^+$ cardiomyocyte labeling by *Kit-CreER* and reassess the differentiation of c-Kit$^+$ non-cardiomyocytes to new cardiomyocytes after injury. We generated *Tnni3-Dre;Kit-CreER;IR1* (DeaLT strategy) and *Kit-CreER;IR1* (conventional strategy) littermates to compare them side-by-side. In *Tnni3-Dre;Kit-CreER;IR1* mice, *Tnni3-Dre* first removes one *lox*P site and ZsGreen from the reporter allele in cardiomyocytes, precluding potential Cre-*lox*P mediated labeling within cardiomyocytes. As a result, if tamoxifen activation of *Kit-CreER* in c-Kit$^+$ non-cardiomyocytes yielded ZsGreen$^+$ cardiomyocytes after cardiac injury, one would conclude that this was due to cardiomyocyte differentiation from c-Kit$^+$ non-cardiomyocytes, rather than labeling of cardiomyocytes themselves (Fig. 2a). To achieve high labeling efficiency, we treated mice with tamoxifen 6 – 8 times between the neonatal and adult stages (Fig. 2b). In adult *Kit-CreER;IR1* hearts, occasional ZsGreen$^+$ cardiomyocytes labeled by *Kit-CreER* were readily observed, in addition to abundant ZsGreen$^+$ endothelial cells (Fig. 2c,d). In contrast, we did not detect ZsGreen$^+$ cardiomyocytes in *Tnni3-Dre;Kit-CreER;IR1* hearts, whereas we continued to observe abundant ZsGreen$^+$ non-myocyte cells (Fig. 2c,d and Supplementary Fig. 4a). Similarly, no ZsGreen$^+$tdTomato$^-$ cardiomyocytes were found after dissociating hearts from *Tnni3-Dre;Kit-CreER;IR1* mice (Supplementary Fig. 4b). Quantitatively, 0.74 ± 0.11% cardiomyocytes were ZsGreen$^+$tdTomato$^-$ in *Kit-CreER;IR1* hearts using the multiple tamoxifen induction strategy (Fig. 2e). However, not a single ZsGreen$^+$tdTomato$^-$ cardiomyocyte was detected after examination of over 500 sections from 4 *Tnni3-Dre;Kit-CreER;IR1* hearts using the same tamoxifen induction strategy (Fig. 2d,e). Taken together, these results demonstrate that, in uninjured hearts, c-Kit$^+$ non-cardiomyocytes do not generate new cardiomyocytes; rather, cardiomyocytes labeled by *Kit-CreER* result from Cre activity in cardiomyocytes, whose substrate is effectively removed by the new strategy.

Although not manifest in uninjured hearts, a latent myogenic potential of c-Kit$^+$ non-cardiomyocytes might be activated by myocardial injury. To test this hypothesis, we performed myocardial infarction (MI) on *Kit-CreER;IR1* and *Tnni3-Dre;Kit-CreER;IR1* mice (Fig. 2b). The control condition was no operation (Fig. 2c–e and Supplementary Fig. 4). Four weeks after coronary artery ligation, we analyzed hearts for expression of the Cre genetic lineage tracer. We observed ZsGreen$^+$tdTomato$^-$ cardiomyocytes in *Kit-CreER;IR1* hearts but not in *Tnni3-Dre;Kit-CreER;IR1* hearts (Fig. 2f). Similarly, no ZsGreen$^+$tdTomato$^-$ cardiomyocytes were found after dissociating hearts (Fig. 2g). Whereas 0.78 ± 0.10% of cardiomyocytes were Cre-labeled (ZsGreen$^+$tdTomato$^-$) in infarcted *Kit-CreER;IR1* hearts, no Cre-labeled cardiomyocytes (ZsGreen$^+$tdTomato$^-$) were observed in more than 500 heart sections examined from 4 infarcted *Tnni3-Dre;Kit-CreER;IR1* hearts (Fig. 2h,i). We observed very rare ZsGreen$^+$tdTomato$^+$ cardiomyocytes (Fig. 2j), consistent with fusion of c-Kit$^+$ cells with cardiomyocytes[16]. These data demonstrate that c-Kit$^+$ non-

cardiomyocytes do not form *de novo* cardiomyocytes after injury (Fig. 2k). Unlike cardiomyocytes, endothelial cells were comparably labeled by the two strategies (Fig. 2l,m).

To independently address the myogenic potential of c-Kit$^+$ non-cardiomyocytes after cardiac injury, we generated a new Dre driver using another cardiomyocyte specific marker, cardiac troponin T2 (*Tnnt2-Dre*, Supplementary Fig. 5a). Like *Tnni3-Dre*, *Tnnt2-Dre* targeted cardiomyocytes specifically and efficiently (Supplementary Fig. 5b,c). Next, we generated a *Tnnt2-Dre;Kit-CreER;IR1* line that permits removal of a *lox*P site in *Tnnt2-Dre* targeted cardiomyocytes (Supplementary Fig. 5d). In both MI and sham heart tissues, we did not detect any ZsGreen$^+$tdTomato$^-$ cardiomyocytes (Supplementary Fig. 5e–g), whereas endothelial cells were efficiently labeled (Supplementary Fig. 5h,i). Taken together, these results indicate that c-Kit$^+$ non-cardiomyocytes do not generate new cardiomyocytes after injury.

Genetic lineage switch uncovered by new strategy

We next asked if the DeaLT-IR strategy is sensitive enough to uncover cell lineage conversion events, by studying as a proof-of-concept the known conversion of hepatocytes into new biliary epithelial cells (BECs) after liver injury[21]. We first generated a mouse line bearing an inducible, hepatocyte-specific Cre, *Alb-CreER* (Supplementary Fig. 6a). After treatment of adult *Alb-CreER;IR1* mice with tamoxifen, we detected the Cre-activated reporter ZsGreen in HNF4a$^+$ hepatocytes but not CK19$^+$ BECs (Supplementary Fig. 6b–d). We next generated a *CK19-Dre* line, which constitutively labeled BECs and also a subset of hepatocytes (Supplementary Fig. 6e–h). Intercrossing yielded *CK19-Dre;Alb-CreER;IR1* mice (DeaLT-IR strategy), in which CK19$^+$ BECs expressed tdTomato and most HNF4a$^+$ hepatocytes were marked by ZsGreen (Fig. 3a). To test if HNF4a$^+$ hepatocytes (ZsGreen$^+$) generate new CK19$^+$ BECs after injury, we exposed *Alb-CreER;IR1* and *CK19-Dre;Alb-CreER;IR1* mice to the liver toxin 3,5-diethoxycarbonyl-1,4-dihydrocollidine (DDC) or bile duct ligation surgery (BDL)[22], and collected livers for analysis before or after injury (Fig. 3b, Supplementary Fig. 7a). After liver injury induced by DDC, there was substantial fibrotic tissue formation (Fig. 3c) and ductal reaction (Fig. 3d). Before DDC treatment, *Alb-CreER* labeled most hepatocytes and did not label any BECs, as no ZsGreen$^+$ BECs were evident using either the conventional or new strategy (Fig. 3e). After DDC-induced injury, a subset of CK19$^+$ BECs expressed ZsGreen using both strategies (Fig. 3f). Quantification of the percentage of ZsGreen$^+$ BECs showed that there was no difference in efficiency of hepatocyte-to-BEC conversion between the conventional and DeaLT-IR strategies (Fig. 3g). Similarly, we found ZsGreen$^+$ BECs in BDL livers (Supplementary Fig. 7b–d), consistent with a previous study[21]. Thus, even with rigorous exclusion of the possibility of unintentional Cre labeling using the new strategy, we detected the Cre hepatic lineage tracer in BECs, indicative of lineage conversion of hepatocytes to biliary epithelial cells (Fig. 3h).

Generation of a nested reporter for two inducible recombinases

The DeaLT-IR strategy using *IR1* reported above requires sequential recombination by Dre-*rox* first and Cre-*lox*P afterwards. However, at times it would be desirable for both Dre and Cre to be under tamoxifen control; for example, during embryonic development, albumin is expressed in hepatoblasts, which give rise to both hepatocytes and BECs[23]. Thus constitutive

Alb-Dre line may target BECs in addition to hepatocytes, reducing its usefulness in distinguishing between the hepatocyte and BEC lineages. To accommodate temporally-controlled Dre-*rox* recombination, we developed a second strategy in which inducible Dre-*rox* recombination controls Cre-mediated lineage tracing. This strategy uses dual recombinases with nested recombinase target sites, so that Dre-*rox* recombination removes *lox*P sites and the Cre-*lox*P readout, preventing Cre-*lox*P mediated lineage tracing, but not the reverse (Fig. 4a,b). To implement this new strategy, we generated a new reporter allele, *n*ested *r*eporter 1 (*NR1*). Unlike the *IR1* reporter that requires sequential recombination, the *NR1* permits simultaneous expression of inducible CreER and DreER recombinases; but similarly to the *IR1* reporter, Dre-*rox* recombination controls Cre-mediated lineage tracing (Fig. 4a,b). As designed, embryos bearing the *NR1* reporter did not express fluorescent protein in the absence of Cre or Dre, expressed tdTomato but not ZsGreen in the presence of *CAG-Dre*, and expressed ZsGreen but not tdTomato in the presence of *ACTB-Cre* (Fig. 4c–e). Having established the *NR1* line, we next used it to address a long-standing debate in liver regeneration.

Sox9$^+$ BECs contribute to ductal cells but not hepatocytes after injury

After liver injury, the ability of Sox9$^+$ BECs to give rise to new hepatocytes to regenerate the liver has been a matter of debate. Recent studies have reached contrasting conclusions, with data showing that Sox9$^+$ liver progenitors contribute to hepatocytes minimally or substantially after injury[24,25]. Whereas Sox9 is highly enriched in BECs, it is also weakly expressed in those hepatocytes that reside close to BECs, referred to as Sox9$^+$ periportal hepatocytes[26]. Since *Sox9-CreER* labels both BECs and a subset of periportal hepatocytes, it has been difficult to resolve whether Sox9$^+$ BECs or Sox9$^+$ hepatocytes give rise to new hepatocytes after injury. To address this question, we generated two inducible recombinase lines, *Alb-DreER* and *Sox9-CreER* (Supplementary Fig. 8a,d). We verified the recombination pattern of *Alb-DreER* and *Sox9-CreER* using *NR1*. After tamoxifen treatment, *Alb-DreER* recombined *NR1* selectively in hepatocytes: ~99.9% HNF4a$^+$ hepatocytes and 0% CK19$^+$ BECs were tdTomato$^+$ZsGreen$^-$ in the liver of *Alb-DreER;NR1* mice (Supplementary Fig. 8b,c). This recombination pattern paralleled *Alb-CreER* activation of a Cre-dependent reporter (Supplementary Fig. 6a–d). Consistent with a previous report[26], *Sox9-CreER* activated *NR1* in the majority of CK19$^+$ BECs but also in a subset of HNF4a$^+$ hepatocytes (Supplementary Fig. 8e,f). Additionally, we generated a *Alb-DreER;R26-rox-tdTomato;Sox9-CreER;R26-loxP-GFP* mouse line, and detected Sox9$^+$Alb$^+$ hepatocytes and Sox9$^+$Alb$^-$ BECs along with Sox9$^-$Alb$^+$ hepatocytes in the liver of these mice (Supplementary Fig. 9). Taken together, these data demonstrate that *Sox9-CreER* labels both BECs and a subset of hepatocytes.

To test if Sox9$^+$ BECs give rise to new hepatocytes after injury, we generated *Alb-DreER;Sox9-CreER;NR1* mice (DeaLT with nested reporter (DeaLT-NR) strategy), as well as *Sox9-CreER;NR1* littermate controls (conventional strategy) for side-by-side comparison. We performed tamoxifen treatment multiple times prior to liver injury, and samples were collected before and after the injury (Fig. 5a). The DeaLT-NR strategy labels Sox9$^+$ BECs with ZsGreen, whereas Sox9$^+$ periportal hepatocytes are labeled by tdTomato due to excision of the Cre-activated reporter ZsGreen by Dre-*rox* recombination (Fig. 5b,c). During

the chase period, if chronic liver injury by CCl_4 induces BECs to differentiate into hepatocytes, we would expect to observe the ZsGreen$^+$tdTomato$^-$ lineage mark in a subset of hepatocytes following injury, but not prior to it. Consistent with published results[26], in pre-injury samples the conventional strategy using *Sox9-CreER;NR1* labeled both BECs and periportal hepatocytes with ZsGreen (Fig. 5d,e and Supplementary Fig. 8f). Quantitatively, 98.21 ± 0.85 % CK19$^+$ BECs and 7.89 ± 1.31% HNF4a$^+$ periportal hepatocytes expressed ZsGreen. Using the DeaLT-NR strategy, in pre-injury samples from *Alb-DreER*;*Sox9-CreER;NR1* mice, 98.82 ± 0.54% CK19$^+$ BECs were labeled by ZsGreen (Fig. 5e). However, no ZsGreen$^+$tdTomato$^-$ HNF4a$^+$ hepatocytes were observed out of >400 liver sections from 4 mice, and >99.9% HNF4a$^+$ hepatocytes were tdTomato$^+$ (Fig. 5e); these results indicate that Dre-*rox* recombination occurred efficiently in hepatocytes, where it abolished unwanted Cre-*lox*P recombination (Fig. 5b–e). Thus, the DeaLT-NR strategy permits specific and efficient genetic labeling of Sox9$^+$ BECs with ZsGreen and HNF4a$^+$ hepatocytes with tdTomato (Fig. 5e). After injury, whole-mount fluorescence imaging showed that the percentage of ZsGreen$^+$ cells labeled by the conventional strategy increased substantially, but this increase was not evident using the DeaLT-NR strategy (Fig. 5d). Immunostaining of injured liver sections labeled by the conventional strategy showed that 99.10 ± 0.53% CK19$^+$ BECs and 15.71 ± 1.62% HNF4a$^+$ hepatocytes expressed ZsGreen. In contrast, using the DeaLT-NR strategy, 99.31 ± 0.34% CK19$^+$ BECs expressed ZsGreen, and no ZsGreen$^+$tdTomato$^-$ HNF4a$^+$ hepatocytes were observed (Fig. 5f). These data indicate that after liver injury, Sox9$^+$ BECs remain BECs and do not undergo a lineage conversion into hepatocytes (Fig. 5g,h).

Resources that expand the use of IR and NR strategies

To expand the application of IR and NR strategies, we generated additional mouse lines harboring reporters that differ in the relative position of recombinase sites and the fluorescent protein readouts. For the IR strategy, in addition to *IR1*, we established *IR2*, *IR3* and *IR4* mouse lines (Fig. 6a). We validated these reporters by activating them with *CAG-Dre* or *ACTB-Cre* (Fig. 6b–g). These mouse reporter lines provide options to best fit the experimental system being studied. For example, some Cre or CreER lines co-express GFP or tdTomato, limiting the choice of the specific lineage-tracing readout. For the NR strategy, we generated another reporter allele *NR2* that permits Cre control of Dre recombinase (Supplementary Fig. 10a). Crossing *NR2* with *CAG-Dre* or *ACTB-Cre* verified that this reporter yields the expected results (Supplementary Fig. 10b–e). These mouse lines provide multiple options for lineage tracing, facilitating the application of the IR and NR strategies to diverse experimental settings.

DISCUSSION

In this study, we developed a new tracing strategy that uses dual recombinases to resolve the uncertainty potentially created by recombinase expression in non-targeted cells. Using interleaved or nested reporter designs, we show that Dre effectively blocks unwanted Cre activity and Cre-reporter readout, thereby clarifying the interpretation of lineage tracing data. We then applied the DeaLT-IR or DeaLT-NR strategies in proof-of-concept studies to address two debates over the plasticity of stem cells in regenerative biology. The first debate

concerns the contribution of c-Kit$^+$ CSCs to the cardiomyocyte lineage[15–17,20]. The observations that c-Kit$^+$ cells in the heart consist of both c-Kit$^+$ cardiomyocytes and c-Kit$^+$ non-cardiomyocytes, and that *Kit-CreER* is expressed in cardiomyocytes during lineage tracing[20], has complicated the interpretation of lineage tracing studies. By taking into account and controlling for *Kit-CreER* activity in cardiomyocytes, we show that c-Kit$^+$ non-cardiomyocytes do not generate new cardiomyocytes in the postnatal heart during homeostasis and after injury. Our lineage tracing study does not directly address the question of whether c-Kit$^+$ cardiomyocytes can contribute to the formation of new cardiomyocytes after cardiac injury, but previous studies have reported that c-Kit$^+$ cells minimally contribute to cardiomyocytes after injury[16,20,27]. Our study focused on adult hearts and does not rule out the cardiomyogenic potential of c-Kit$^+$ CSCs in fetal hearts, as suggested by a recent study reporting that c-Kit$^+$ CSCs originating from neural crest possess full cardiomyogenic capacity at embryonic stages[28].

Second, we resolved the long-standing question on whether Sox9$^+$ hepatic progenitors differentiate into new hepatocytes during liver regeneration. Using conventional Cre-*lox*P lineage tracing, previous studies were unable to determine the extent to which Sox9$^+$ BEC-to-hepatocyte conversion occurs, because *Sox9-CreER* labels both Sox9$^+$ BECs and a subset of periportal hepatocytes. Using our new strategy, we were able to label and trace Sox9$^+$ BECs distinctly, and avoid tracing of pre-existing Sox9$^+$ hepatocytes. Our data support the conclusion that Sox9$^+$ BECs adopt a ductal cell but not hepatocyte fate after injury, whereas Sox9$^+$ hepatocytes expand to generate new hepatocytes, consistent with previous studies[24,29,30].

To achieve selective lineage tracing, previous studies have used an intersectional recombinase strategy. Several alleles designed for an intersectional approach have been reported, including *R26::FLAP*[31], *RC::FrePe*[28,32], *RC::Fela*[28,33], *RC::RLTG*[34,35]. For these reporters, recombination by two different recombinases labels cells in which both recombinases are active with a distinct reporter, distinguishing them from cells labeled by only one of the recombinases. Similarly, we found that Cre and Dre drivers and their corresponding reporter alleles, when combined together in a single mouse, can distinguish single- from double-positive recombinase cells (Supplementary Fig. 9). The current study adds a new set of reporters that enrich this rapidly evolving field for more precise lineage tracing (Supplementary table 1). Among these reporters, the interleaved set is unique because it reports on the temporal sequence of recombination, unlike the intersectional and nested strategies. In comparing the intersectional and nested strategies, the intersectional strategy is optimal for identifying cells in which both recombinases are active, whereas the nested strategy is designed to identify cells in which one recombinase and not the other is active (for *NR1*, Cre but not Dre is active; for *NR2*, Dre but not Cre is active). Compared with single recombinase-mediated tracing, utilization of dual recombinases and their corresponding reporters enable more stringent, accurate and sophisticated fate-mapping studies.

The IR or NR strategy not only provides more precise control of Cre recombinase and sets a higher technical standard for lineage tracing of Cre-expressing cells, but also is sensitive enough to detect positive lineage-conversion events *in vivo*. Using hepatocyte to BEC

conversion in liver injury as an example, our IR strategy was able to clearly demonstrate *in vivo* conversion of hepatocytes to BECs. Thus, this new strategy can be used to uncover cell fate switches while also rigorously controlling for potential non-targeted Cre-mediated lineage tracing.

As with any recombinase system, there are caveats to the use of these new lineage tracing strategies. In this study, we refer to a cell lineage as a population of cells that is labeled by a recombinase system. These population level studies do not address the question of the types of cells that arise from individual precursor cells, which would require study of the clonal derivatives of individual precursors. However, we note that the recombinase systems described in this study could be used for clonal analyses.

The DeaLT-IR and DeaLT-NR systems require a Cre mouse line, a Dre mouse line, and the appropriate reporter line. Since we have already generated and validated several reporters, and Cre lines are often widely available, application of these new strategies will typically require generation of a Dre mouse line (Supplementary Fig. 11a). We propose that when a positive lineage result is detected by single recombinase-mediated tracing but there is uncertainty regarding the expression of Cre or the gene that drives Cre, our systems could be used for further fate mapping. A robust promoter should be selected to drive Dre or DreER, because incomplete or inefficient recombination by Dre or DreER would not fully preclude unintentional Cre-*lox*P recombination in Dre-expressing cells. Inclusion of the Woodchuck hepatitis virus post-transcriptional regulatory element (WPRE) after Dre cDNA could be considered for the purpose of stabilizing Dre-encoding mRNA and elevating Dre protein levels, which might result in greater recombination efficiency. Furthermore, the specificity of the genetic elements available to express Dre in Cell B is critical to the overall experimental design and to the choice of Dre or DreER: if promoter B is specific to Cell B throughout all stages of development, the use of Dre and an interleaved reporter would be most effective, but if promoter B is specific only within a given time window, then use of DreER and a nested reporter are recommended (Supplementary Fig. 11a).

In summary, taking advantage of established and widely-used Cre-*lox*P based genetic tools, we have developed the DeaLT-IR and DeaLT-NR strategies to permit unambiguous determination of the contribution of one genetic lineage to another. These strategies are intended to reduce ambiguity in lineage tracing studies caused by uncertainty as to whether Cre is expressed in pre-existing, non-targeted cells (Supplementary Fig. 11b). These new strategies and reagents provide the means to more precisely dissect cell origin and fate, without invasive manipulation or cell transplantation[36–38], in multiple fields of research.

ONLINE METHODS

Detailed information on experimental design and reagents can be found in the Life Sciences Reporting Summary.

Mice.

All mouse studies were carried out in strict accordance with the guidelines of the Institutional Animal Care and Use Committee (IACUC) at the Institute for Nutritional

Sciences, Shanghai Institutes for Biological Sciences, Chinese Academy of Sciences. *CAG-Dre*, *ACTB-Cre*, *UBC-CreER*, *αMHC-MerCreMer*, *Kit-CreER*, *R26-loxP-tdTomato*, *R26-rox-tdTomato*, *R26-GFP* mouse lines were reported previously[12,20,39–43]. The interleaved reporter 1 (*IR1*) knock-in mouse line was generated by knocking CAG-*lox*P-*rox*-Stop-*lox*P-ZsGreen-polyA-*rox*-tdTomato-polyA-Frt-Neo-Frt into the Rosa26 locus, as previously described[44]. Two homologous arms on the 5' and 3' sides of intron 1 of Rosa26 were generated in targeting vectors by recombination; the targeting vector was then linearized and electroporated into mouse ES cells. After G418 selection, approximately 200 clones were selected for retrieval of genomic DNA and for screening of positive clones. Neomycin-resistant clones were tested for correct gene targeting by long PCR assays with primer pairs spanning the targeting vector and flanking genomic DNA. Following verification of correct targeting and karyotype, at least 2 positive ES clones were expanded and injected into blastocysts for mouse generation. The obtained chimera mouse lines were crossed to C57BL/6J lines for germline transmission. PCR primers spanning the genomic DNA and inserted cassette were designed to test the correct genotype. Chimeric mice positive for targeted ES cells were germline transferred to the F1 generation and bred on a C57/B6; ICR background. Similarly, we generated the *IR2* mouse line by knocking the CAG-*lox*P-*rox*-Stop-*lox*P-tdTomato-Stop-*rox*-ZsGreen-polyA-Frt-Neo-Frt cassette into the Rosa26 locus; the *IR3* mouse line by knocking the CAG-*rox*-*lox*P-Stop-*rox*-tdTomato-Stop-*lox*P-ZsGreen-polyA-Frt-Neo-Frt cassette into the Rosa26 locus; the *IR4* mouse line by knocking the CAG-*rox*-*lox*P-Stop-*rox*-ZsGreen-polyA-*lox*P-tdTomato-Stop-Frt-Neo-Frt cassette into the Rosa26 locus; the *NR1* mouse line by knocking the Rosa26-CAG-*rox*-*lox*p-Stop-*lox*p-ZsGreen-Stop-*rox*-tdTomato-polyA-frt-Neo-frt cassette into the Rosa26-locaus; and the *NR2* mouse line by knocking the Rosa26-CAG-*lox*p-*rox*-Stop-*rox*-ZsGreen-Stop-*lox*p-tdTomato-polyA-frt-Neo-frt cassette into the Rosa26 locus. For these Stop sequences, the first Stop sequence is triple SV40 polyA sequences and the second Stop sequence is adapted from the polyA sequence between mT and mG of pCA-mTmG (Addgene #26123). The *Alb-CreER* knock-in mouse line was generated by knocking Cre recombinase and estrogen receptor fusion protein cDNA into the translational start cordon of the Alb gene. Briefly, A 129 mouse BAC clone containing the complete mouse Alb gene was obtained from the Sanger Institute (UK). A targeting vector was constructed containing the following cassettes: $CreER^{T2}$ cDNA, SV40 polyA sequence and Frt sites-flanked PGK-EM7-Neo resistant gene. Two homologous arms on 5' and 3' sides of first coding exon of Alb gene were generated in targeting vectors by recombination from the BAC. The targeting vector was digested with I-CeuI for linearization and then electroporated into mouse ES cells. The targeting vector containing the aforementioned cassettes was knocked into the Alb locus for endogenous expression of $CreER^{T2}$ cDNA. After G418 selection, approximately 200 clones were selected for retrieval of genomic DNA and for screening of positive clones. Neomycin-resistant clones were tested for correct gene targeting by long PCR assays with primer pairs spanning the targeting vector and flanking genomic DNA. Following verification of correct targeting and karyotype, at least 2 positive ES clones were expanded and injected into blastocysts for mouse generation. The obtained chimera mouse lines were then crossed to C57BL/6J lines for germline transmission. PCR was carried out to test the correct genotype and the established *Alb-CreER* mouse lines were maintained on a C57BL/6J; ICR background. *Tnni3-Dre*, *Tnnt2-Dre*, *CK19-Dre*, *Sox9-CreER*, *Alb-DreER and CAG-DreER*

knock-in mouse lines were generated by genome editing using CRISPR/Cas9 technology as previously described[45]. A cDNA encoding Dre recombinase was inserted into the translational start codon of the Tnni3 or CK19 gene; a cDNA encoding CreER^{T2} recombinase was inserted after the translational stop codon of the Sox9 gene; a cDNA encoding DreER^{T2} recombinase was inserted after the translational stop codon of the Alb gene; and a cDNA encoding DreER^{T2} recombinase was inserted into the Rosa26 locus. To strengthen the stability of transcripts, we included the Woodchuck hepatitis virus posttranscriptional regulatory element (WPRE) before the polyA signal sequence. The *IR1*, *IR2*, *NR1*, *NR2*, *CAG-DreER*, *Tnni3-Dre*, *Tnnt2-Dre*, *Alb-CreER*, *CK19-Dre* and *Alb-DreER* mouse lines were generated by Shanghai Model Organisms Center, Inc. (SMOC). The *IR3* and *IR4* mouse lines were generated by the Nanjing Biomedical Research Institution of Nanjing University, Nanjing, China. *Sox9-CreER* was generated by National Institute for Biological Sciences, Beijing, China. For induction of CreER-*lox*P or DreER-*rox* recombinations, tamoxifen (Sigma, T5648) was dissolved in corn oil (20 mg/ml) and administered by gavage at the indicated time points (0.1–0.15 mg tamoxifen/g mouse body weight) as described previously[46]. Both male and female mice were used and were randomized into different treatment groups in all experiments.

Genomic PCR.

Genomic DNA was prepared from embryonic yolk sac or mouse tail. Tissues were lysed by incubation with lysis buffer (100 mM Tris HCl (pH 7.8), 5 mM EDTA, 0.2% SDS, 200 mM NaCl and 100 μg/ml proteinase K) overnight at 55°C, followed by centrifugation at maximum speed (21,130*g*) for 5 minutes to obtain supernatant with genomic DNA. DNA was precipitated by isopropanol, washed in 70% ethanol and dissolved in deionized water. All embryos and mice were genotyped using genomic PCR as described previously[47].

Whole mount fluorescence microscopy.

Mouse hearts or embryos were washed in phosphate-buffered saline (PBS), and fixed in 4% paraformaldehyde at 4°C for 20 minutes to 1 hour depending on tissue size, followed by PBS washing 3 times. Tissues were placed on an agar gel for whole mount bright-field or fluorescence imaging using a Zeiss stereo microscope (AxioZoom V16).

Immunostaining.

Immunostaining was performed as previously described[48]. Briefly, embryos or hearts were collected in PBS on ice and then fixed in 4% PFA at 4 °C for 20 minutes to 1 hour depending on tissue size. After washing in PBS for three times, tissues were dehydrated in 30% sucrose/PBS overnight at 4 °C, then embedded in optimum cutting tissue (O.C.T, Sakura) and stored at −80°C until sectioning. Cryosections 10 μm in thickness were collected on positively charged slides and stored at −20 °C until use. For immunostaining, tissue sections were blocked with PBSST (0.1% Triton X-100/2.5% normal donkey serum/PBS) for 30 minutes at room temperature, followed by primary antibody incubation overnight at 4 °C. The next day, tissue sections were washed with PBS for three times and incubated with Alexa fluorescence-conjugated secondary antibodies (Invitrogen) for 30 minutes at room temperature, then washed with PBS three times and mounted with mounting medium containing DAPI (Vector Lab). For weak signals, we used horseradish

peroxidase or biotin-conjugated secondary antibodies and a tyramide signal amplification kit (PerkinElmer). The antibodies used were as follows: tdTomato (Rockland, 600-401-379; 1:1,000 dilution), TNNI3 (Abcam, ab56357; 1:100 dilution), CDH5 (R&D, AF1002; 1:100 dilution), PECAM (BD Pharmingen, 553370; 1:500 dilution), αSMA (Sigma, F3777; 1:500 dilution), PDGFRa (eBioscience, 14-1401-81; 1:500 dilution), CK19 (DSHB, TROMA-III; 1:500 dilution), HNF4a (Santa Cruz, sc-6556; 1:100 dilution), GFP (Abcam, ab6662; 1:100 dilution). ZsGreen polyclonal antibody was obtained from immunized rabbits, and characterized by immunostaining on $ZsGreen^+$ tissue samples. Immunostaining images were acquired using an Olympus confocal microscope (FV1200), Leica confocal (TCS SP5), or a Zeiss stereo microscope (AxioZoom V16). To provide *Z*-stack images, 5–10 consecutive *XY* images were scanned on the *Z* axis using Olympus confocal microscope. The obtained images were analyzed by ImageJ (NIH) software. The images were merged using the Image color-merge channels function, and the Z-stack images were performed using *Z*-stack function in Image J with average intensity projection of each image taken serially in Z axis. In the stack, an orthogonal view was used to reveal the signals on the *XZ* or *YZ* axes. Merged signals and split channels were used to delineate the signals at single cell resolution, as described previously[41].

Quantification of labeled cardiomyocytes and endothelial cells.

Mouse hearts were collected and embedded for serial coronal section. For each adult heart, all the collected sections were put on 52 to 65 positively charged slides, 6 slides as a set, and each slide contained 8 – 10 heart sections. Slides were stained with TNNI3 and ZsGreen. The percentage of labeled cardiomyocytes was calculated as the number of $ZsGreen^+TNNI3^+$ cardiomyocytes divided by the number of $TNNI3^+$ cardiomyocytes. A researcher who was blinded to the groups quantified the percentage using an Olympus fluorescence microscope (BX53). Labeling of endothelial cells was quantified as the percentage of $ZsGreen^+CDH5^+$ endothelial cells in $CDH5^+$ endothelial cells. At least 4 hearts per group were quantified.

Myocardial infarction in adult mice.

Adult mice of 9–12 weeks were subjected to surgical manipulation as described previously[49]. Briefly, mice on a heated pad were anaesthetized with 2% isoflurane gas through tracheal intubation. When the mouse did not respond to tail and toe pinch, its limbs were fixed on the pad and its chest was disinfected by iodine. A vertical 1 cm incision was made at the chest skin, and a blunt dissection of the muscle and fascia was performed to avoid injuring the blood vessels. After making a 1 cm incision between the third and fourth intercostal ribs, the internal chest was exposed for subsequent operation. Then the LAD branch of the coronary artery was permanently ligated with a 0–8 suture. The ligation was judged to be successful when the heart showed signs of cyanosis. The incision was closed with a 6–0 suture, and air was discharged from the chest. The surgical incision was disinfected and mice were supplied with pure oxygen for 4–5 minutes until they resumed spontaneous breathing. Then the tracheal intubation tube was removed and the mice were kept warm until recovery of normal behavior, followed by treatment with analgesics. In the sham operation group, the same procedure was followed but ligation of the LAD coronary

artery was omitted. The person who performed the surgery was blinded to the allocation of different experimental groups.

Cardiomyocyte isolation.

Adult cardiomyocytes were isolated as described previously[20]. Briefly, adult mice were injected with 200μl heparin (6.25 U/μl) intraperitoneally to prevent coagulation of blood in the coronary arteries. Twenty minutes later, the mice were anesthetized with pentobarbital sodium at 80mg/kg body weight by intraperitoneal injection, followed by an interval of 5–10 minutes until the mice stopped responding to tail and toe pinches. Then the hearts were dissected and ligated to a perfusion fluid-filled aortic cannula, and were perfused with perfusion buffer (NaCl 137mM, KCl 4mM, NaH_2PO_4 0.33mM, MgCl2 1mM, HEPES 10mM, Taurine 5mM, BDM 10mM, Glucose 10mM, pH 7.4) at a flow rate of 4 ml/min for approximately 5 minutes, until the effluent became clear. Perfusion liquid was switched to digestion buffer (Perfusion buffer containing 0.1mg/μl Collagenase II and 0.08mg/μl Protease XIV) and perfused for 12–15 minutes at the same flow rate. The digested hearts were transferred to transfer buffer (Perfusion buffer containing 0.5mg/ml BSA), minced by forceps and filtered through a 100μm strainer. The isolated cells were centrifuged for 3 minutes at 20x g to pellet cardiomyocytes, which were subsequently re-suspended in transfer buffer for further analysis.

Liver injury models.

5-diethoxycarbonyl-1,4-dihydrocollidine (DDC), carbon tetrachloride (CCl_4) and bile duct ligation (BDL) were used as liver injury models. All of the liver injury models were carried out after at least 2 weeks tamoxifen washout time. For DDC chronic liver injury model, adult mice of 11 weeks were given 0.1% wt/wt DDC (Sigma-Aldrich) in PMI Mouse Diet (#5015, Harlan Teklad) for 8 weeks; control mice were fed with PMI Mouse diet. For the CCl_4 chronic liver injury model, CCl_4 was dissolved in corn oil (1:3) first, then the mice of 11 weeks were given CCl_4 (1ul/g) by intraperitoneal injection once every 3 days for a total of 15 injections. Control mice received the equivalent amount of corn oil. BDL injury model was carried out according to established protocols[50]. Adult mice of 11 weeks were anaesthetized with 2% isoflurane gas in a sealed chamber. Then the abdominal fur was removed and the skin was disinfected by iodine. The mice were transferred onto a 37°C heating pad and anesthesia was maintained by inhalation of isoflurane. A midline abdominal incision was made to expose the liver. The common bile duct was ligated twice with 4–0 silk sutures. After the ligation, the skin incisions were closed with a 6–0 suture, and the mice were supplied with pure oxygen for 4–5 minutes until they resumed normal breathing. Then the tracheal intubation tube was removed and the mice were kept warm until recovery of normal behavior. In the sham operation group, the same procedure was followed, except the common bile duct was not ligated.

Statistics.

All data were determined from 3 – 4 independent experiments as indicated in each figure legend and presented as mean values ± s.e.m. All mice were randomly assigned to different experimental groups. Statistical comparisons between data sets were made with analysis of

normality and variance. A two-sided unpaired Student's *t* test was used for comparing differences between two groups. The null hypothesis was rejected if *P* was < 0.05.

Supplementary Material

Refer to Web version on PubMed Central for supplementary material.

ACKNOWLEDGMENTS

We thank B. Wu, G. Chen, Z. Weng and A. Huang for the animal husbandry; and W. Bian for technical help. We thank H. Zeng at Allen Institute for sharing mice lines and K. Anastassiadis for valuable suggestions and insightful advice on this study. This work was supported by Strategic Priority Research Program of the Chinese Academy of Sciences (CAS, XDB19000000), The National key Research & Development Program of China (2017YFC1001303 and 2016YFC1300600), National Science Foundation of China (31730112, 91639302, 31625019, 31571503, 31501172, 31601168, 31701292), Youth Innovation Promotion Association of CAS (2015218), Key Project of Frontier Sciences of CAS (QYZDB-SSW-SMC003), International Cooperation Fund of CAS, National Program for Support of Top-notch Young Professionals, Shanghai Science and Technology Commission (17ZR1449600, 17ZR1449800), Young Elite Scientists Sponsorship Program by China Association for Science and Technology, Shanghai Yangfan Project (15YF1414000, 16YF1413400) and Rising-Star Program (15QA1404300), China Postdoctoral Science Foundation, President Fund of Shanghai Institutes for Biological Sciences (SIBS), Astrazeneca, Sanofi-SIBS Fellowship, Boehringer Ingelheim and Royal Society-Newton Advanced Fellowship.

References

1. Laugwitz KL et al. Postnatal isl1+ cardioblasts enter fully differentiated cardiomyocyte lineages. Nature 433, 647–653 (2005). [PubMed: 15703750]
2. Smart N et al. De novo cardiomyocytes from within the activated adult heart after injury. Nature 474, 640–644 (2011). [PubMed: 21654746]
3. Chen Q et al. Endothelial cells are progenitors of cardiac pericytes and vascular smooth muscle cells. Nat Commun 7, 12422 (2016). [PubMed: 27516371]
4. Kumar ME et al. Mesenchymal cells. Defining a mesenchymal progenitor niche at single-cell resolution. Science 346, 1258810 (2014). [PubMed: 25395543]
5. Snippert HJ et al. Intestinal crypt homeostasis results from neutral competition between symmetrically dividing Lgr5 stem cells. Cell 143, 134–144 (2010). [PubMed: 20887898]
6. Klotz L et al. Cardiac lymphatics are heterogeneous in origin and respond to injury. Nature 522, 62–67 (2015). [PubMed: 25992544]
7. Sauer B & Henderson N Site-specific DNA recombination in mammalian cells by the Cre recombinase of bacteriophage P1. Proc Natl Acad Sci U S A 85, 5166–5170 (1988). [PubMed: 2839833]
8. Nagy A Cre recombinase: the universal reagent for genome tailoring. Genesis 26, 99–109 (2000). [PubMed: 10686599]
9. Davis J, Maillet M, Miano JM & Molkentin JD Lost in Transgenesis: A User's Guide for Genetically Manipulating the Mouse in Cardiac Research. Circ Res 111, 761–777 (2012). [PubMed: 22935533]
10. Tian X, Pu WT & Zhou B Cellular Origin and Developmental Program of Coronary Angiogenesis. Circ Res 116, 515–530 (2015). [PubMed: 25634974]
11. Sauer B & McDermott J DNA recombination with a heterospecific Cre homolog identified from comparison of the pac-c1 regions of P1-related phages. Nucleic Acids Res 32, 6086–6095 (2004). [PubMed: 15550568]
12. Anastassiadis K et al. Dre recombinase, like Cre, is a highly efficient site-specific recombinase in E. coli, mammalian cells and mice. Dis Model Mech 2, 508–515 (2009). [PubMed: 19692579]
13. Guo C, Yang W & Lobe CG A Cre recombinase transgene with mosaic, widespread tamoxifen-inducible action. Genesis 32, 8–18 (2002). [PubMed: 11835669]
14. Beltrami AP et al. Adult cardiac stem cells are multipotent and support myocardial regeneration. Cell 114, 763–776 (2003). [PubMed: 14505575]

15. Ellison GM et al. Adult c-kit(pos) Cardiac Stem Cells Are Necessary and Sufficient for Functional Cardiac Regeneration and Repair. Cell 154, 827–842 (2013). [PubMed: 23953114]
16. van Berlo JH et al. c-kit+ cells minimally contribute cardiomyocytes to the heart. Nature 509, 337–341 (2014). [PubMed: 24805242]
17. Hatzistergos KE et al. Stimulatory Effects of MSCs on cKit+ Cardiac Stem Cells Are Mediated by SDF1/CXCR4 and SCF/cKit Signaling Pathways. Circ Res 119, 921–930 (2016). [PubMed: 27481956]
18. Molkentin JD & Houser SR Are Resident c-Kit+ Cardiac Stem Cells Really All That Are Needed to Mend a Broken Heart? Circ Res 113, 1037–1039 (2013). [PubMed: 24115067]
19. Molkentin JD Letter by Molkentin regarding article, “The absence of evidence is not evidence of absence: the pitfalls of Cre Knock-Ins in the c-Kit Locus”. Circ Res 115, e21–3 (2014). [PubMed: 25258403]
20. Liu Q et al. Genetic lineage tracing identifies in situ Kit-expressing cardiomyocytes. Cell Res 26, 119–130 (2016). [PubMed: 26634606]
21. Yanger K et al. Robust cellular reprogramming occurs spontaneously during liver regeneration. Genes Dev 27, 719–724 (2013). [PubMed: 23520387]
22. Pu W et al. Mfsd2a+ hepatocytes repopulate the liver during injury and regeneration. Nat Commun 7, 13369 (2016). [PubMed: 27857132]
23. Zorn AM & Wells JM Vertebrate endoderm development and organ formation. Annu Rev Cell Dev Biol 25, 221–251 (2009). [PubMed: 19575677]
24. Tarlow BD, Finegold MJ & Grompe M Clonal tracing of Sox9+ liver progenitors in mouse oval cell injury. Hepatology 60, 278–289 (2014). [PubMed: 24700457]
25. Furuyama K et al. Continuous cell supply from a Sox9-expressing progenitor zone in adult liver, exocrine pancreas and intestine. Nat Genet 43, 34–41 (2011). [PubMed: 21113154]
26. Font-Burgada J et al. Hybrid Periportal Hepatocytes Regenerate the Injured Liver without Giving Rise to Cancer. Cell 162, 766–779 (2015). [PubMed: 26276631]
27. Sultana N et al. Resident c-kit(+) cells in the heart are not cardiac stem cells. Nat Commun 6, 8701 (2015). [PubMed: 26515110]
28. Hatzistergos KE et al. cKit+ cardiac progenitors of neural crest origin. Proc Natl Acad Sci U S A 112, 13051–13056 (2015). [PubMed: 26438843]
29. Carpentier R et al. Embryonic ductal plate cells give rise to cholangiocytes, periportal hepatocytes, and adult liver progenitor cells. Gastroenterology 141, 1432–8, 1438.e1 (2011). [PubMed: 21708104]
30. Yanger K et al. Adult hepatocytes are generated by self-duplication rather than stem cell differentiation. Cell Stem Cell 15, 340–349 (2014). [PubMed: 25130492]
31. Awatramani R, Soriano P, Rodriguez C, Mai JJ & Dymecki SM Cryptic boundaries in roof plate and choroid plexus identified by intersectional gene activation. Nat Genet 35, 70–75 (2003).
32. Engleka KA et al. Islet1 derivatives in the heart are of both neural crest and second heart field origin. Circ Res 110, 922–926 (2012). [PubMed: 22394517]
33. Jensen P et al. Redefining the serotonergic system by genetic lineage. Nat Neurosci 11, 417–419 (2008). [PubMed: 18344997]
34. Plummer NW et al. Expanding the power of recombinase-based labeling to uncover cellular diversity. Development 142, 4385–4393 (2015). [PubMed: 26586220]
35. Plummer NW, de Marchena J & Jensen P A knock-in allele of En1 expressing dre recombinase. Genesis 54, 447–454 (2016). [PubMed: 27313055]
36. Wang X et al. Cell fusion is the principal source of bone-marrow-derived hepatocytes. Nature 422, 897–901 (2003). [PubMed: 12665832]
37. Alvarez-Dolado M et al. Fusion of bone-marrow-derived cells with Purkinje neurons, cardiomyocytes and hepatocytes. Nature 425, 968–973 (2003). [PubMed: 14555960]
38. Vassilopoulos G, Wang PR & Russell DW Transplanted bone marrow regenerates liver by cell fusion. Nature 422, 901–904 (2003). [PubMed: 12665833]
39. Ruzankina Y et al. Deletion of the developmentally essential gene ATR in adult mice leads to age-related phenotypes and stem cell loss. Cell Stem Cell 1, 113–126 (2007). [PubMed: 18371340]

40. Sohal DS et al. Temporally regulated and tissue-specific gene manipulations in the adult and embryonic heart using a tamoxifen-inducible Cre protein. Circ Res 89, 20–25 (2001). [PubMed: 11440973]
41. Liu Q et al. c-kit(+) cells adopt vascular endothelial but not epithelial cell fates during lung maintenance and repair. Nat Med 21, 866–868 (2015). [PubMed: 26168292]
42. Madisen L et al. A robust and high-throughput Cre reporting and characterization system for the whole mouse brain. Nat Neurosci 13, 133–140 (2010). [PubMed: 20023653]
43. Zhang H et al. Endocardium Contributes to Cardiac Fat. Circ Res 118, 254–265 (2016). [PubMed: 26659641]
44. Zhang H et al. Endocardium Minimally Contributes to Coronary Endothelium in the Embryonic Ventricular Free Walls. Circ Res 118, 1880–1893 (2016). [PubMed: 27056912]
45. Zhang H et al. Genetic lineage tracing identifies endocardial origin of liver vasculature. Nat Genet 48, 537–543 (2016). [PubMed: 27019112]
46. Liu Q et al. Genetic targeting of sprouting angiogenesis using Apln-CreER. Nat Commun 6, 6020 (2015). [PubMed: 25597280]
47. Tian X et al. Subepicardial endothelial cells invade the embryonic ventricle wall to form coronary arteries. Cell Res 23, 1075–1090 (2013). [PubMed: 23797856]
48. He L et al. Genetic lineage tracing discloses arteriogenesis as the main mechanism for collateral growth in the mouse heart. Cardiovasc Res 109, 419–430 (2016). [PubMed: 26768261]
49. Zhou B et al. Adult mouse epicardium modulates myocardial injury by secreting paracrine factors. J Clin Invest 121, 1894–1904 (2011). [PubMed: 21505261]
50. Tag CG et al. Bile Duct Ligation in Mice: Induction of Inflammatory Liver Injury and Fibrosis by Obstructive Cholestasis. JoVE (2015).

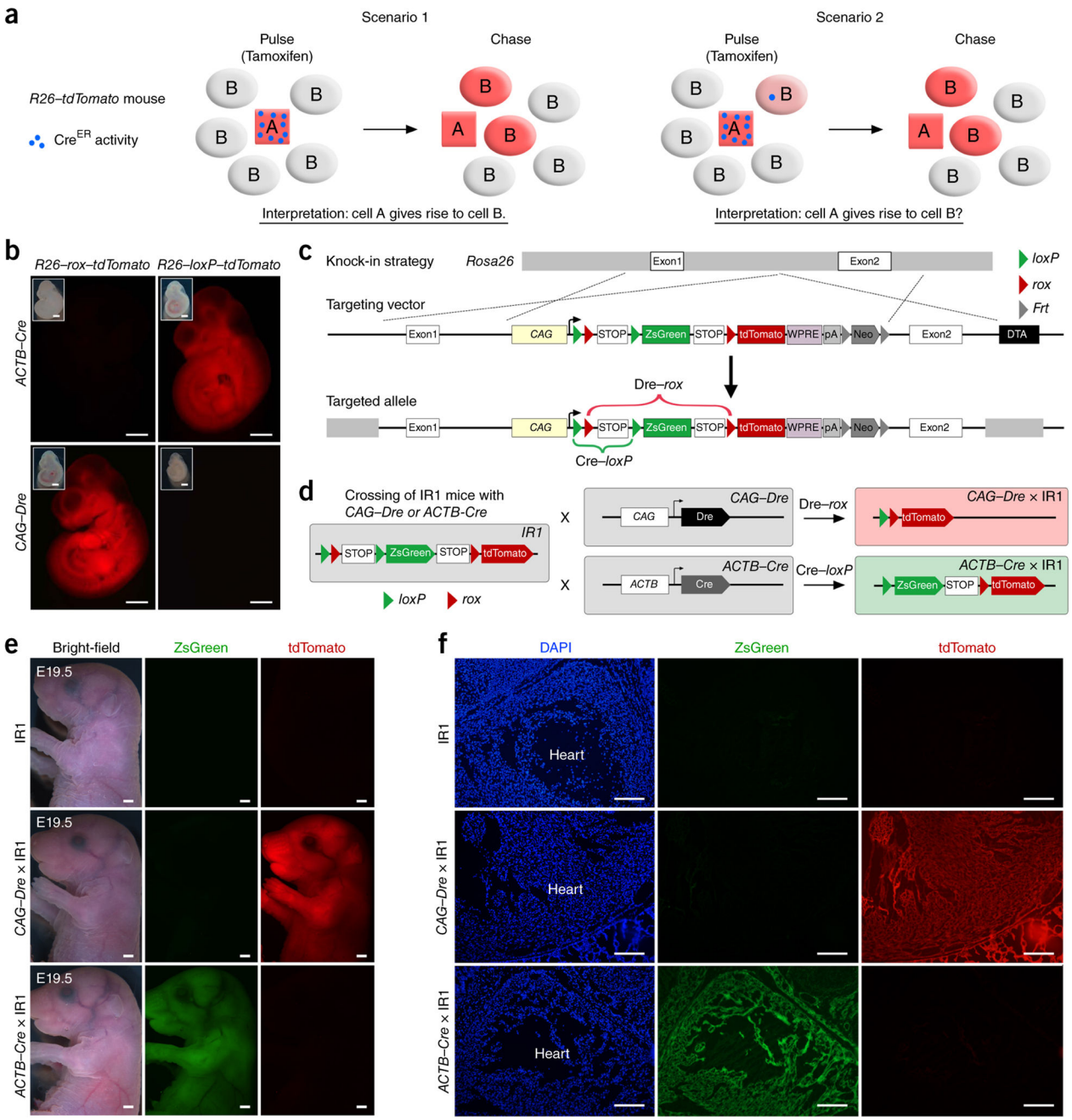

Figure 1.

Generation and characterization of an interleaved reporter (*IR1*). (**a**) Schematic showing how Cre activity in unintended cell types confounds lineage tracing. In Cell A that expresses CreER, Cre-*lox*P recombination results in tdTomato expression when the mouse is treated with tamoxifen (“Pulse”). After a period of time (“Chase”), Cell B is found to express tdTomato. The conclusion that Cell B derives from Cell A is based on the absence of CreER expression in Cell B (scenario 1). Expression of CreER in Cell B, even at trace levels, may lead to Cre-*lox*P recombination in Cell B and labeling of Cell B, even if Cell A does not generate Cell B (scenario 2). As a result, unintended labeling of Cell B makes interpretation

that Cell A gives rise to Cell B uncertain in scenario 2. (**b**) Recombination results, as assessed by tdTomato expression, for combinations of Cre and Dre drivers (*ACTB-Cre* and *CAG-Dre*) and *rox* and *lox*P reporters (*R26-rox-tdTomato* and *R26-loxP-tdTomato*) in E9.5 embryos. (**c**) Schematic showing how the *IR1* reporter allele was generated by homologous recombination. DTA, diphtheria toxin; Neo, neomycin; pA, polyA sequence; Frt, Frt sequence as a substrate of Flp recombinase; WPRE, Woodchuck hepatitis virus posttranscriptional regulatory element. (**d**) Schematic diagram showing the result of Dre-*rox* or Cre-*lox*P recombination after crossing the *IR1* mouse line with *CAG-Dre* or *ACTB-Cre* lines. (**e**) Whole mount bright-field and epifluorescent images showing ZsGreen and tdTomato staining in *IR1*, *CAG-Dre;IR1* and *ACTB-Cre;IR1* E19.5 embryos. (**f**) Immunostaining for ZsGreen and tdTomato in embryos as in **e**. DAPI was used as a nuclear stain. The location of the heart is indicated. Scale bars, 1 mm in **b**,**e**; 200 μm in **f**. Each figure is representative of 4 individual mouse samples.

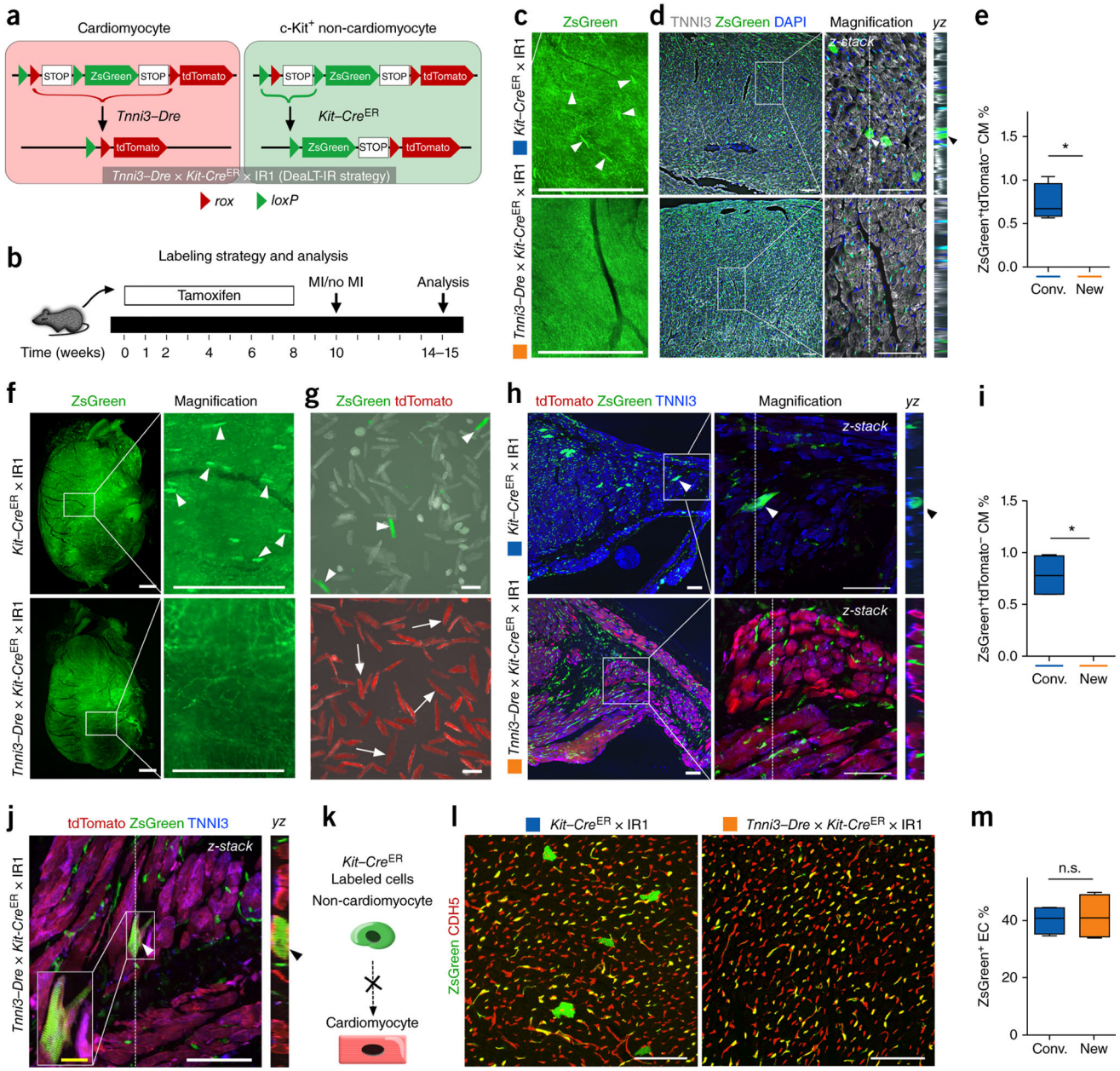

Figure 2.

c-Kit^{+} non-cardiomyocytes do not generate cardiomyocytes. (**a**) Schematic showing the DeaLT-IR strategy for lineage tracing of c-Kit^{+} non-cardiomyocytes (ZsGreen^{+}). See text for details. (**b**) Schematic showing the experimental timeline. After Tam administration, the mice were subjected to MI or no operation. (**c,d**) Whole-mount epifluorescence (**c**) and sectional staining for ZsGreen, TNNI3 and DAPI (**d**) in uninjured hearts from *Kit-CreER;IR1* and *Tnni3-Dre;Kit-CreER;IR1* mice. Magnification indicates white boxed region in images of left panel (d). YZ indicate signals from dotted lines on magnified *Z*-stack images. Arrowheads indicate cardiomyocytes. (**e**) Quantification of the percentage of ZsGreen^{+}tdTomato^{-} cardiomyocytes. Conv., conventional strategy; New, new strategy. *$P <$ 0.05; n = 4 per group. (**f**) Whole-mount fluorescence of infarcted hearts from *Kit-CreER;IR1*

and *Tnni3-Dre;Kit-CreER;IR1* mice. Arrowheads indicate cardiomyocytes. (**g**) Fluorescence images of cardiomyocytes dissociated from *Kit-CreER;IR1* (top) and *Tnni3-Dre;Kit-CreER;IR1* hearts (bottom). Arrowheads indicate *Kit-CreER* labeled cardiomyocytes; arrows indicate *Tnni3-Dre* labeled cardiomyocytes. (**h**) Immunostaining for tdTomato, ZsGreen and TNNI3 in heart sections of the indicated mice. *YZ* indicates signals from *Z*-stack images along the orthogonal plane indicated by dotted lines. Arrowheads indicate a cardiomyocyte. (**i**) Quantification of the percentage of $ZsGreen^{+}tdTomato^{-}$ cardiomyocytes. $*P < 0.05$; n = 4 per group. (**j**) Immunostaining for tdTomato, ZsGreen and TNNI3 in a section from the heart of a *Tnni3-Dre;Kit-CreER;IR1* mouse shows a $tdTomato^{+}ZsGreen^{+}$ cardiomyocyte (arrowhead), suggesting that cell fusion occurred between c-Kit^{+} cell ($ZsGreen^{+}$) and cardiomyocyte ($tdTomato^{+}$). (**k**) Schematic figure showing that c-Kit^{+} non-cardiomyocytes do not generate cardiomyocytes after injury. (**l**) Immunostaining for ZsGreen and CDH5 in sections from the hearts of the indicated mice. (**m**) Quantification of the percentage of $ZsGreen^{+}$ endothelial cells. n.s., non-significant; n = 4 per group. Scale bars, 1 mm in c,f; 100 μm in d,g,h,j,l. Each figure is representative of 4 individual mouse samples.

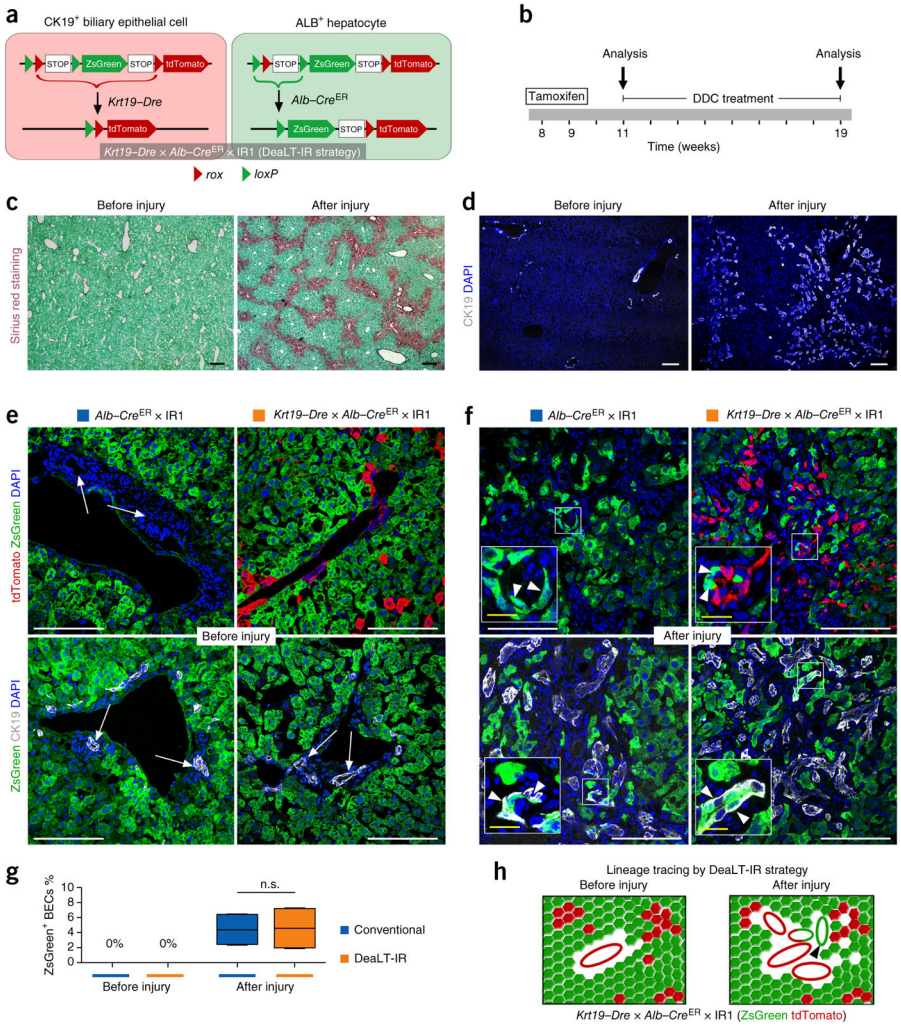

Figure 3.

Hepatocyte-to-ductal cell conversion uncovered by DeaLT-IR strategy. (**a**) Schematic showing tdTomato labeling of CK19$^+$ biliary epithelial cells (BECs) by Dre-*rox* recombination. After tamoxifen induction, Alb$^+$ hepatocytes but not BECs will be ZsGreen-labeled by Cre-*lox*P recombination. (**b**) Schematic showing the experimental timeline for cell labeling with Tam, injury by DDC treatment, and analysis. (**c,d**) Sirius red staining to assess fibrosis (**c**) and CK19 immunostaining to assess the ductal reaction (**d**) of liver sections of *CK19-Dre;Alb-CreER;IR1* mice before and after injury. (**e,f**) Immunostaining for ZsGreen with tdTomato (top) or with CK19 (bottom) of liver sections from *Alb-CreER;IR1* (conventional strategy) or *CK19-Dre;Alb-CreER;IR1* (DeaLT-IR strategy) mice before (**e**) and after (**f**) injury. *Alb-CreER* labels hepatocytes but not BECs (arrows) before injury. After injury, a few ZsGreen$^+$ cells (arrowheads) exhibit ductal cell-like morphology and express the BEC marker CK19. (**g**) Quantification of the percentage of ZsGreen$^+$ BECs before and after injury, as determined using each of the two strategies. n = 4 per group. (**h**) Cartoon showing that a subset of new BECs (arrowhead) is derived from ZsGreen$^+$ hepatocytes after injury. Scale bars, 200 μm in c; 100 μm in d-f. Each figure is representative of 4 individual mouse samples.

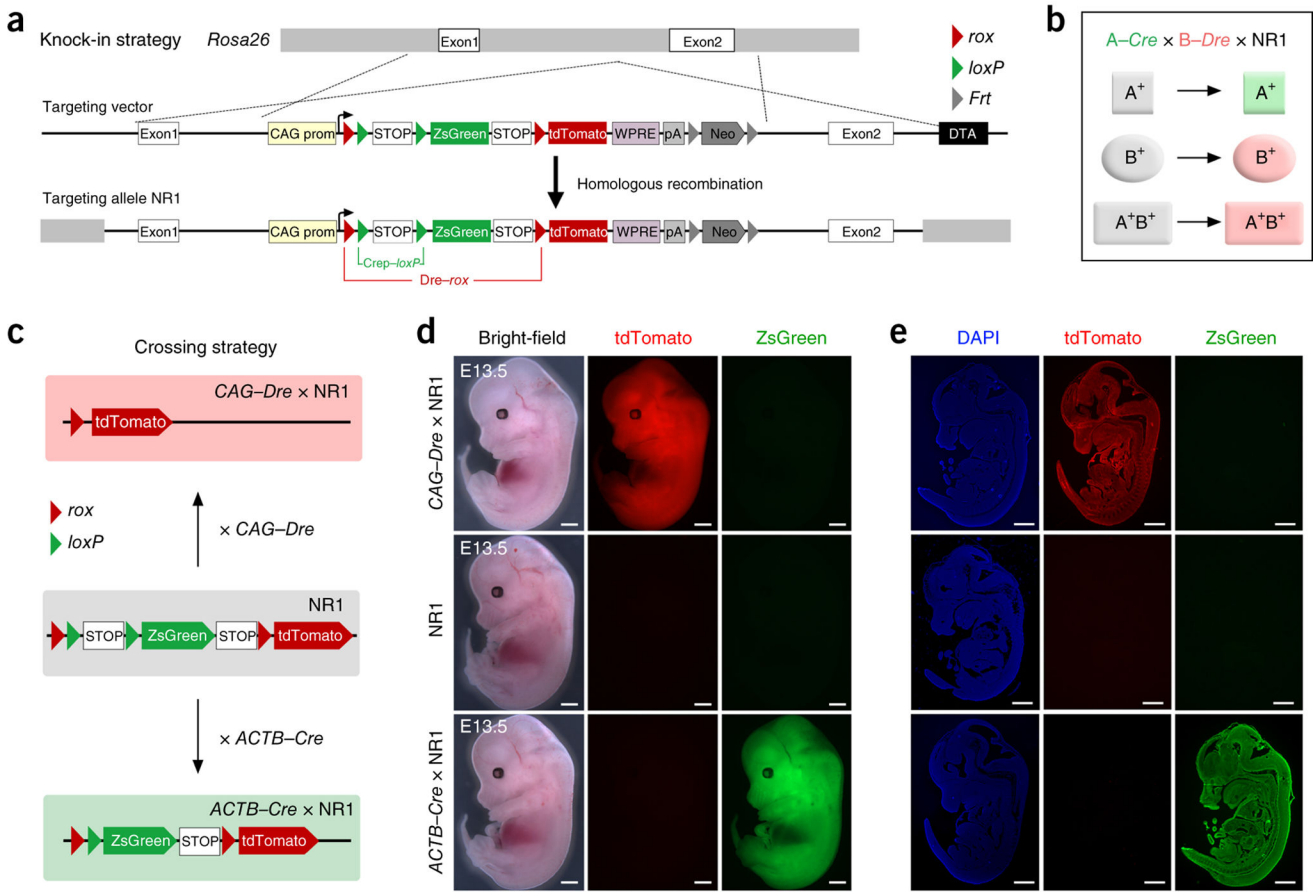

Figure 4.

Generation and characterization of a secondary dual reporter system that uses nested recombinase sites. (**a**) Schematic showing the strategy for generation of the *NR1* allele by homologous recombination. (**b**) Cartoon showing the pattern of cell labeling using the *A-Cre;B-Dre;NR1* strategy. A^+ cells express Cre under control of the A promoter; B^+ cells express Dre under control of the B promoter; A^+B^+ cells express both Dre and Cre. This strategy labels A^+ cells by ZsGreen, B^+ cells by tdTomato, and A^+B^+ cells by tdTomato. (**c**) Schematic showing the strategy for crossing of *CAG-Dre* or *ACTB-Cre* mouse lines with the *NR1* line. (**d**) Whole-mount bright-field and epifluorescence images of E13.5 *NR1*, *CAG-Dre;NR1* and *ACTB-Cre;NR1* embryos. (**e**) Immunostaining for tdTomato and ZsGreen on sections of embryos as in **d**. Scale bars, 1 mm. Each figure is representative of 4 individual mouse samples.

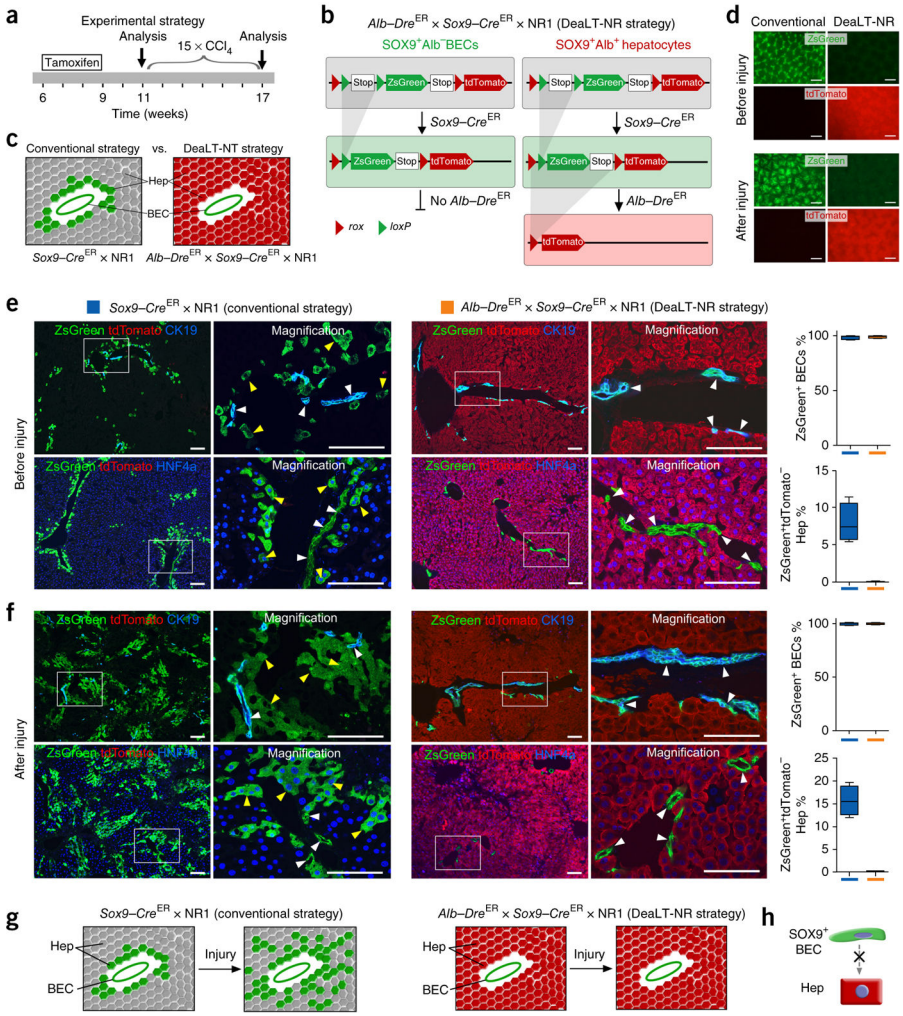

Figure 5.

Sox9$^+$ biliary epithelial cells adopt a ductal cell but not a hepatocyte fate after injury. (**a**) Schematic showing the experimental timeline for cell labeling with Tam, injury with CCl_4, and analysis (**b**) Schematic showing the patterns of Cre- and Dre-mediated recombination in BECs and hepatocytes of *Alb-DreER;Sox9-CreER;NR1* mice. (**c**) Cartoon showing the differences in how BECs and hepatocytes (Hep) are labeled by the conventional strategy (*Sox9-CreER;NR1*) and by the DeaLT-NR strategy (*Alb-DreER;Sox9-CreER;NR1*). (**d**) Whole-mount fluorescence for ZsGreen and tdTomato in liver before and after injury, using either the conventional or DeaLT-NR strategies. (**e,f**) Immunostaining for ZsGreen, tdTomato, CK19 and HNF4a before (**e**) or after (**f**) injury in sections of livers labeled by either the conventional (left) or DeaLT-NR (right) strategies. White arrowheads indicate BECs; yellow arrowheads indicate hepatocytes. Quantification of ZsGreen$^+$ BECs or hepatocytes (Hep) is shown. n = 4 per group. (**g**) Cartoon showing the result of *Sox9-CreER* fate mapping by the two strategies. (**h**) Cartoon image showing that Sox9$^+$ BECs do not generate new hepatocytes. Scale bars, 500 μm in d; 100 μm in e, f. Each figure is representative of 4 individual mouse samples.

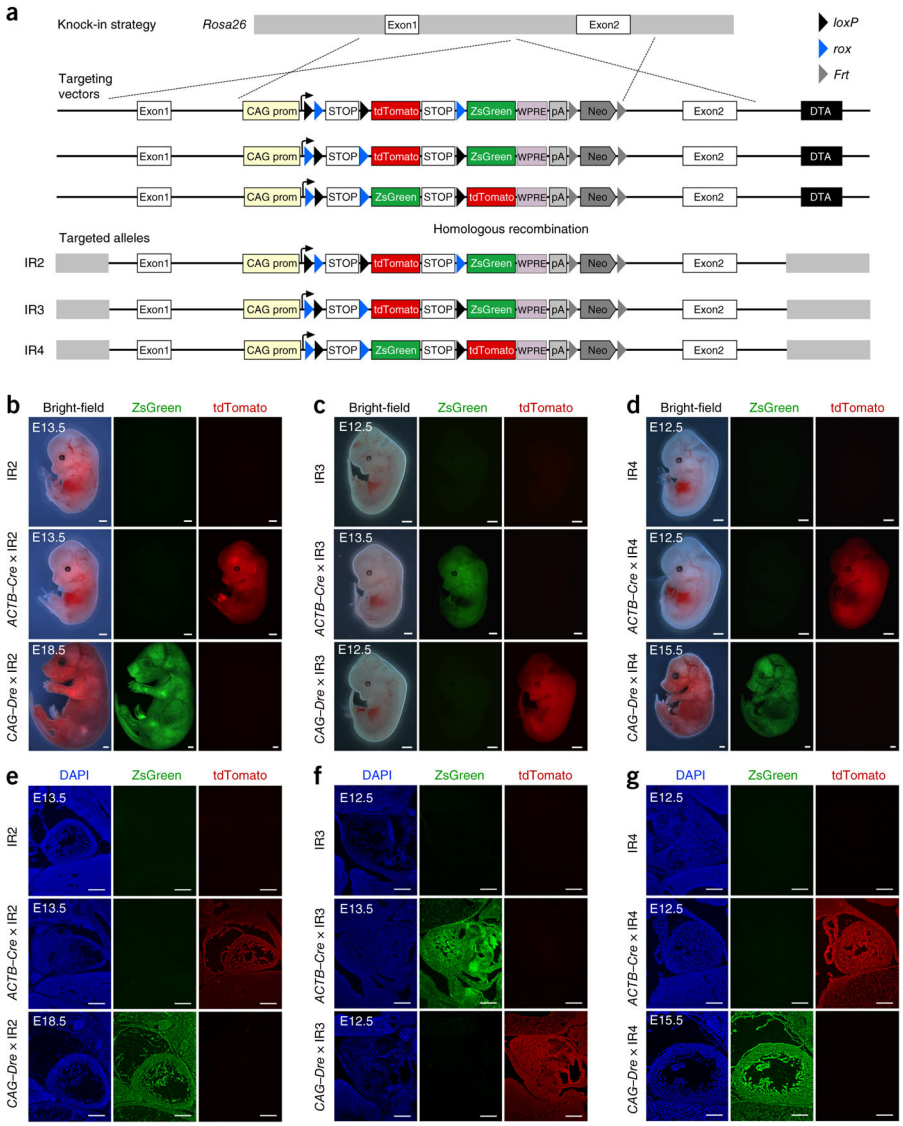

Figure 6.

Generation and characterization of additional interleaved reporter alleles. (**a**) Schematic figure showing the knockin strategy for generation of the alleles *IR2*, *IR3* and *IR4* by homologous recombination. (**b-d**) Whole-mount bright-field and epifluorescence images of mouse lines bearing the *IR2* (**b**), *IR3* (**c**) and *IR4* (**d**) reporter alleles; these lines were crossed with the *ACTB-Cre* or *CAG-Dre* lines, as indicated. Embryo ages are indicated. (**e-g**) Immunostaining for ZsGreen and tdTomato in sections of embryos as in **b-d**. Scale bars, 1 mm in b-d; 200 μm in e-g. Each image is representative of 3 individual embryonic samples.